Journal of Materials Chemistry A

Accepted Manuscript

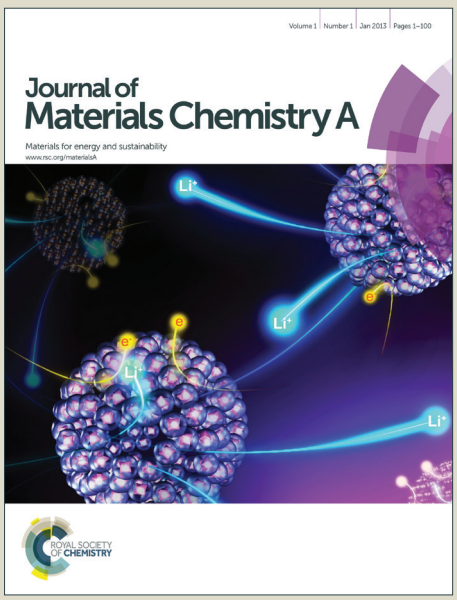

ROYAL SOCIETY OF CHEMISTRY

www.rsc.org/materialsA

Cite this: DOI: 10.1039/c0xx00000x

www.rsc.org/xxxxxx

ARTICLE TYPE

A coordination chemistry approach for shape controlled synthesis of indium oxide nanostructures and its photoelectrochemical properties

Dipak V. Shinde,[a] Do-young Ahn,[a] Vijaykumar A. Jadhav,[b] Deok Yeon Lee,[a] Nabeen K Shrestha,[a] Joong Kee Lee,[c] Hwa Young Lee,[c] Rajaram S. Mane[b] and Sung-Hwan Han*[a]

Received (in XXX, XXX) Xth XXXXXXXXX 20XX, Accepted Xth XXXXXXXXX 20XX
DOI: 10.1039/b000000x

Indium oxide (In_2O_3) is an important wide band-gap semiconductor having applications in variety of optoelectronic devices. We report here, on the low temperature solution deposition of $In(OH)_3$ and $In(SO_4)(OH).H_2O$ architectures with various shapes such as Cubes, maize corns and giant crystals. The In_2O_3 nanostructures are then obtained by solid state transformation of $In(OH)_3$ and $In(SO_4)(OH).H_2O$ architectures. Shape control is achieved by controlling the local concentration of In^{+3} ions available for reaction by applying the principles of coordination chemistry, thereby obviating the need of any shape controlling agents. The phase and surface composition is obtained by X-ray diffraction (XRD) and X-ray photoelectron spectroscopy (XPS) measurements. The XPS is used to probe the defect structure of In_2O_3 architectures. Optical properties of the films, studied by UV-Vis absorption and photoluminescence (PL) spectroscopy measurements, show that the different morphologies have different band-gaps. Furthermore current-voltage characteristics of In_2O_3-CdSe photoelectrochemical cells are studied, which show that Cubes-CdSe samples show excellent photovoltaic behaviour, exhibiting short circuit current density in excess of 10 mA/cm^2. The charge transport properties of the In_2O_3-CdSe photoanodes are studied by impedance spectroscopy show that Cubes-CdSe samples have lowest resistance for charge transfer.

Introduction

Semiconductor nanostructures have attracted considerable attention in recent years due to their exceptional properties compared to their bulk counterparts and their application in optoelectronics.[1] In_2O_3 is one such semiconductor having a band gap of about ~3 eV. It has unique optical, chemical and electrical properties and is used in variety of applications like batteries, thin film infrared reflectors transparent for visible light (hot mirrors), non-linear optics, nanoelectronics, gas sensing, biosensing, photoelectrochemical cells and antistatic coatings.[2] In combination with tin dioxide, indium oxide forms indium-tin-oxide (also called tin-doped indium oxide or ITO), a material used for transparent conductive coatings. The physico-chemical properties of nanocrystalline semiconductors depend strongly on their morphology. Various methods employed for fabricating indium oxide nanostructures include electrodeposition, chemical bath deposition, chemical vapor deposition, molecular beam epitaxy, hydrothermal, sol-gel synthesis method etc.[3] Among these methods, chemical deposition is the simplest and low cost method with simple setup for deposition. In wet chemical synthesis, for controlling the shape of nanocrystals, a variety of shape controlling agents are used such as, complexing agents, surfactants and P^H regulating agents. All these additives make the synthesis method complicated and costly. Furthermore these additives can act as impurities, thereby lowering the performance of the device in which they are employed. In_2O_3 nano/micro structures with different morphologies like nanorods, cubes, donouts, spheres, porous microspheres, nanoplates, nanorombohedra, flowers etc have been synthesized by various methods.[3] Some reports have shown that catalytic, gas sensing and photoelectrochemical properties have strong dependence on the morphology and electronic defect structure of In_2O_3.[2f,4] Wide band-gap oxides like TiO_2, SnO_2, ZnO etc have been extensively studied for their application in dye and semiconductor sensitized solar cells.[1a,5] However, despite of favorable band positions, ideal band-gap and stability in wide range of electrolytes, reports on successful photosensitization of In_2O_3 are rare.[6] Therefore, controlling the morphology and defect structure remains a key issue in developing high performance photoelectrochemical cells using In_2O_3. To address this, we report here a soft chemical strategy for shape controlled synthesis of indium hydroxide/ sulfate hydroxide hydrate architectures, without using any morphology controlling agents. By applying the principles of co-ordination chemistry and using Pearson's acid-base concept as a guiding principle, we were able to synthesize three different morphologies viz. cubes, maize corns and crystals. Furthermore, these architectures were transformed into In_2O_3 architectures (Scheme 1). These architectures were then sensitized with CdSe nanoparticles to form In_2O_3-CdSe heterostructures, which were utilized in photoelectrochemical cells. Photocurrent in excess of 10 mA/cm^2 was obtained with

Cite this: DOI: 10.1039/c0xx00000x

www.rsc.org/xxxxxx

ARTICLE TYPE

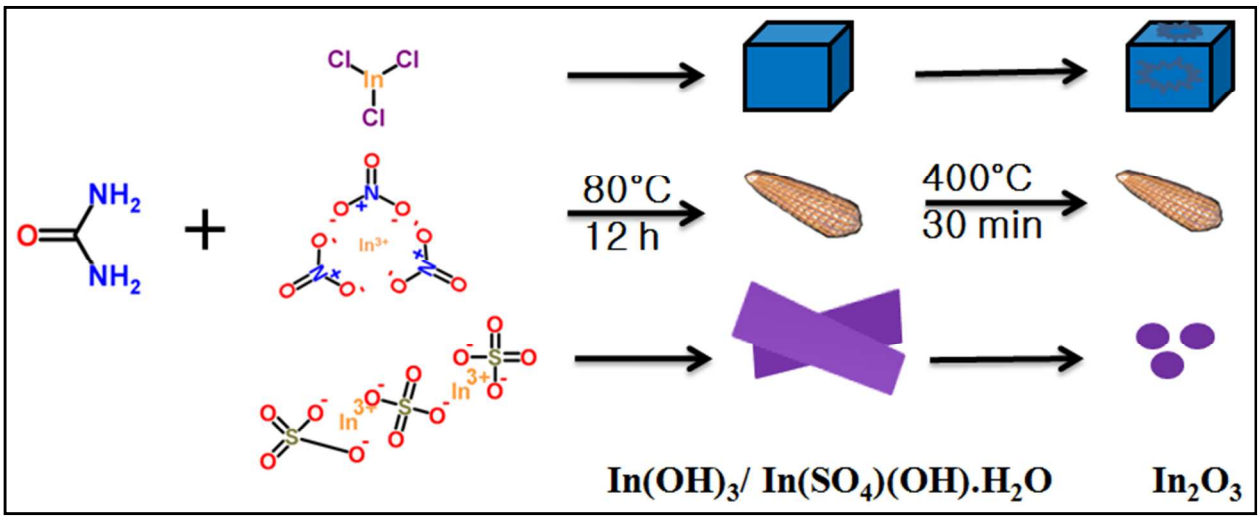

Scheme 1 A schematic representation of the reaction between various indium ion precursors like $InCl_3$, $In(NO_3)_3$, $In_2(SO_4)_3$ and urea in aqueous medium. The $InCl_3$ and $In(NO_3)_3$, upon reaction with urea form $In(OH)_3$ cubes and maize corns respectively while, indium sulphate forms micron sized crystals of $In(SO_4)(OH).H_2O$. On annealing in air at 400 °C, these architectures get transformed into In_2O_3.

Cubes-CdSe photoelectrochemical cells under 1 Sun illumination. To the best of our knowledge, this is the first report on chemical solution deposition of In_2O_3 on conducting substrates with different morphologies and highest performance obtained using In_2O_3 as transparent n-type oxide in sensitized solar cells.

Experimental

All the reagents used in this experiment were of analytical grade, obtained from Aldrich chemical co. and used without further purifications. The FTO coated glass slides (7.5*2.5 cm^2) used for the deposition were cleaned successively with detergent, isopropanol and acetone ultrasonically and finally dried with a stream of air. In a typical experiment, 0.1 M each of Indium nitrate, Indium chloride and Indium sulphate were separately dissolved in 25 mL of deionized water in falcon tubes of 50 mL capacity. To each of these solutions, 25 mL of 0.3 M Urea solution was added. The tubes were then sealed and kept in a water bath maintained at 80 °C. After completion of reaction (evidenced by white deposits on the walls of tubes) after 12 h, the tubes were taken out of the bath, allowed to cool and the films covered with white coating of Indium hydroxide/ sulphate hydroxide hydrate were washed with water, dried in a stream of air and stored for further characterizations.

In_2O_3 architectures were obtained by annealing the samples in muffle furnace at 400 °C for 30 min. After annealing, the colour of sample changed from white to faint yellow, indicating the formation of In_2O_3. For photoelectrochemical cells, the CdSe was deposited onto In_2O_3 architectures by chemical bath deposition. The deposition bath consisted of 80 mM cadmium sulphate, 90 mM nitro tri-acetic acid disodium salt, and 80 mM sodium selenosulfate solution. The In_2O_3 architectures on FTO were

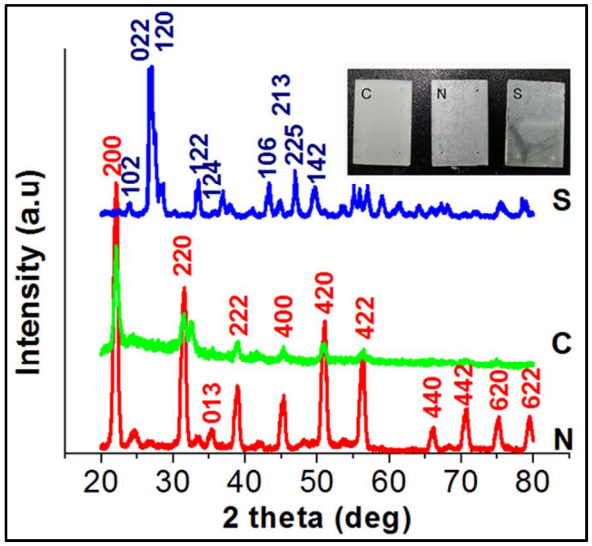

Fig. 2 X-ray diffraction patterns of $In(OH)_3$ (N, C) and $In(SO_4)(OH).H_2O$ (S) architectures fabricated from various indium ion sources such as indium nitrate (N), chloride(C) and sulphate (S). Inset shows the digital photoimages of the corresponding films on FTO substrates.

dipped in the deposition solution and kept at 40 °C in a water bath for 3h. The films coated with CdSe nanoparticles were then taken out, washed with deionized water, dried in a stream of air and annealed in air at 250 °C for 30 min.

The crystal structure and phase of the architectures were confirmed using X-ray diffractometer (Rigaku D/MAX 2500 V, Cu Kα, λ =0.15418 nm). The morphology of the architectures was monitored using a field emission-scanning electron

Cite this: DOI: 10.1039/c0xx00000x

www.rsc.org/xxxxxx

ARTICLE TYPE

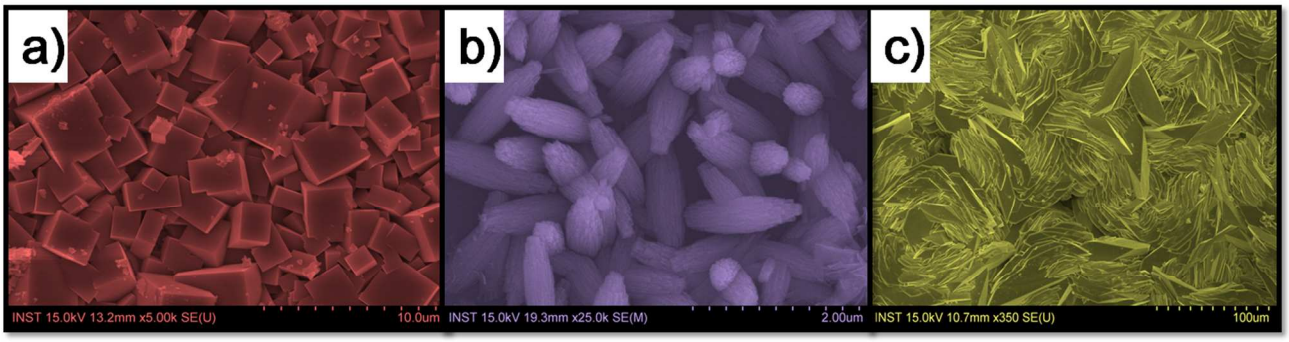

Fig. 3 False colour scanning electron microscope images of the indium hydroxide (a, b) and indium sulphate hydroxide hydrate (c) architectures fabricated on FTO substrates from different indium ion precursors.

microscope (FE-SEM, Hitachi S-4200). UV–Vis absorption spectra were recorded on a spectrophotometer (CARY 100 conc-EL04073168) with another identical reference FTO substrate. XPS spectra were obtained using twin Mg K-alpha source at a chamber base pressure of ~10^{-10} Torr. In order to measure the solar-to-electric power conversion efficiency, In_2O_3-CdSe heterostructures on FTO were incorporated into a thin layer sandwich-type cells with a Pt-coated FTO as the counter electrode (obtained by sputtering), using a spacer film (50 µm thick polyester film) and an electrolyte, 0.1 M polysulfide. Cell performance was measured by irradiation with 100 mW/cm^2 white light (1 Sun) with Air Mass (AM) 0 and 1.5 filters as a solar simulator in the presence of a water filter (450 W xenon lamp, Oriel Instruments). Impedance spectra of the same cells were measured with an IVIUM Compactstat impedance analyser, under open circuit conditions. The AC frequency range was 0.1 to 10^6 Hz with sinusoidal amplitude of 50 mV. Impedance parameters were obtained by fitting the obtained curves using Z-view software. Photoelectrochemical properties of pristine In_2O_3 electrodes were measured in a three electrode cell using In_2O_3 coated FTO as working, Ag/AgCl(3M NaCl) as reference and platinum wire as counter electrode. The working electrode was contacted with a copper back-plate and then pressed against an O-ring in the base of an electrochemical cell, leaving an area of 0.38 cm^2 exposed to the electrolyte. The electrolyte was 1M NaOH solution in deionized water. The samples were then illuminated with simulated 1 Sun radiation through the electrolyte. Linear sweep voltammograms were measured using an Ivium compactstat, at a sweep rate of 10 mV/s.

Results and Discussion

Pearson's acid-base concept classifies metal ions and ligands into hard and soft category.[7] Hard acids prefer to bind to hard bases and vice-versa. We utilized this concept, in the present study to control the shape of the nanoarchitectures. We chose three different In^{3+} ion precursors, viz. $In(NO_3)_3$, $InCl_3$ and $In_2(SO_4)_3$. In the present case, the basicity of ligands is in the order of Cl^- > SO_4^{2-} > NO_3^- while In^{3+} ion is a hard acid. Thus, it is clear that, In^{3+} ions will bind more preferentially to Cl^- ions and less with NO_3^- ions; while intermediate to SO_4^{2-} ions. This factor will in turn affect the local concentration of In^{3+}ions available for the reaction, which consequently will be shape determining factor for indium oxide architectures. Complexing agents or surfactants used for shape control of nanostructures have similar role of controlling the local concentration of metal ions or anions available for the reaction. Thus implying the principles of co-ordination chemistry one can control the shape of the nano architectures, thereby obviating the need of any complexing agents or surfactants. Urea was used as source of hydroxide ions in the present study, which decomposes slowly in aqueous solution at higher temperature to produce hydroxide ions according to the following reaction

$$NH_2CONH_2 + 3H_2O \rightarrow 2NH_4OH + CO_2 \quad (1)$$

These formed hydroxide ions then react with the In^{3+} ions in the

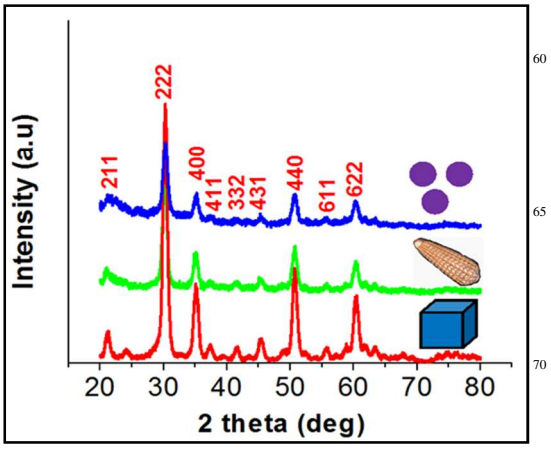

Fig. 4 X-ray diffraction patterns of indium oxide architectures of different morphologies obtained by thermal decomposition of indium hydroxide and indium sulfate hydroxide hydrate films on glass substrates.

Cite this: DOI: 10.1039/c0xx00000x

www.rsc.org/xxxxxx

ARTICLE TYPE

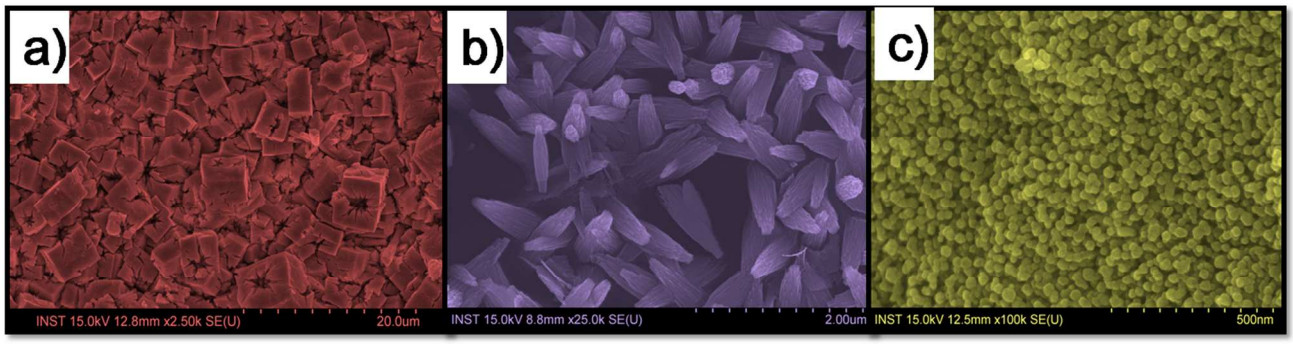

Fig. 5 False colour scanning electron microscope images of the indium oxide architectures obtained by thermal decomposition of indium hydroxide and indium sulfate hydroxide hydrate architectures on FTO substrates.

solution to produce different architectures according to the mechanism discussed above. The possible reaction mechanism leading to the formation of different architectures with different In^{3+} ions precursors can be given as below:

$$InCl_3 + 3OH^- \rightarrow In(OH)_3 + 3Cl^- \quad (2)$$

$$In(NO_3)_3 + 3OH^- \rightarrow In(OH)_3 + 3NO_3^- \quad (3)$$

$$In_2(SO_4)_3 + OH^- + H_2O \rightarrow 2In(SO_4)(OH).H_2O + SO_4^- \quad (4)$$

The hydroxide ions formed by hydrolysis of the urea at high temperature react with the indium ions to precipitate indium hydroxide architectures in case of indium nitrate and chloride, whereas, in case of Indium sulphate, indium sulphate hydroxide hydrate is produced. It has been proven that, indium exists as sufato complex in aqueous indium sulphate solutions. Digital photoimages of the samples formed on FTO substrates are shown in inset of fig. 2. Fairly uniform deposits can be confirmed from the image. The XRD patterns of the indium hydroxide and sulphate hydroxide hydrate products are shown in fig.2. The diffraction patterns of the products synthesized from indium nitrate termed as N and chloride termed as C precursors, match with the a body-centered cubic (bcc) $In(OH)_3$ with a lattice constant a = 7.979 Å (JCPDS card no.85-1338), while that synthesized from indium sulfate termed as S, match with $In(SO_4)(OH).H_2O$ with a lattice constant a = 6.058 (JCPDS card no. 14-0608). The sharp diffraction patterns in case of N, as compared to C products indicate higher crystallinity of the former, which was further confirmed from SEM measurements. The S products also have strong reflection peaks indicating high crystallinity. SEM images of the products are shown in fig. 3. Cuboids of edge lengths of 2-8 micron corresponding to sample N can be seen in the image A. The angle between adjacent edges looks close to 90°, consistent with cubic shape. These cuboids are packed well in the film form and look well interconnected to each other. This can be beneficial in a sense that, many applications, including solar cells, sensors, supercapacitors etc need the material in thin film form with good interconnectivity and conductivity. Furthermore, cubic particles expose a specific surface, which provides an ideal model for the study of surface related properties. Qiu et al. reported the fabrication of cubic particles of indium hydroxide by hydrothermal route using sodium borohydride and polyvinyl pyrrolidone.[8] Our method produces the particles directly on the conducting glass substrates at relatively low temperatures without the use of any surfactant. Maize corn like structures can be seen in case of sample C, which we can assume that, are formed from many small nanorods joined together. These structures are 1-2 micron in length, while the diameters range from 100-150 nm on the top to 500-600 nm in the middle (body). Some structures seem to be growing from the body of other substrates, while others are growing from FTO substrates. In case of sample S, large crystals of 80-90 µm dimensions can be seen. Additional low resolution SEM images of the samples are shown in fig. S1. In a further experiment, we transformed the above architectures into indium oxide architectures by thermal annealing at 400 °C. As reported in the literature, indium hydroxide undergoes solid state transformation to indium oxide, upon annealing at 400 °C.[8] Upon annealing, all the films changed the color from white to faint yellow, indicating the formation of indium oxide. This was further confirmed from XRD measurements. After annealing, all the samples showed reflections corresponding to the cubic phase of indium oxide with a lattice constant of a = 10.11 Å, consistent with JCPDS Card No. 71-2194. The intensity of the reflection peaks was highest in case of cube samples, as compared with corn and particle samples. The cubes and corn samples retain the high crystallinity even after annealing and transformation to indium oxide. Thus, after conversion to indium oxide, the indium hydroxide particles maintain the crystallinity order. In case of indium sulfate hydroxide hydrate particles, after annealing, the reflection peaks become much weaker, which is attributed to formation of nanoparticles of small size (explained later in the text) by complete destruction of original crystals. The chemical equations for solid state transformation can be given as below,

$$2In(OH)_3 \rightarrow In_2O_3 + 3H_2O \quad (5)$$

$$2In(SO_4)(OH).H_2O \rightarrow In_2O_3 + 3H_2O + 2SO_3 \quad (6)$$

The SEM images of indium oxide products formed after solid

Cite this: DOI: 10.1039/c0xx00000x

www.rsc.org/xxxxxx

ARTICLE TYPE

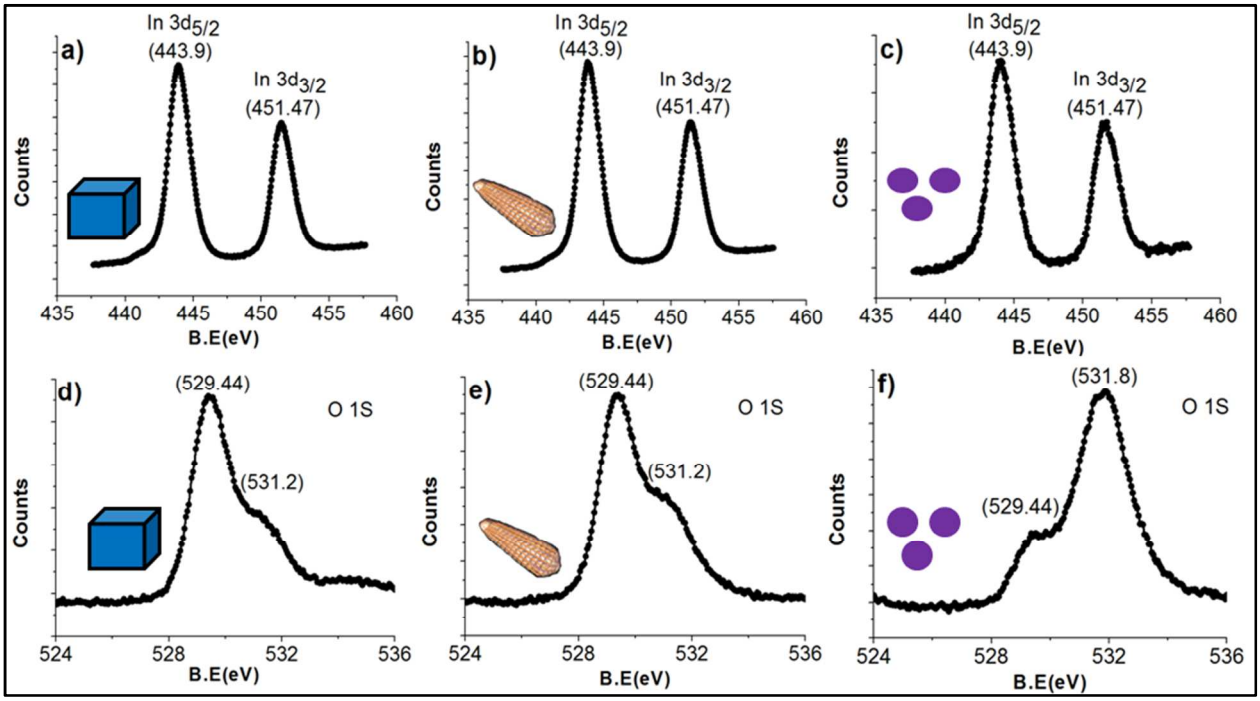

Fig. 6 In3d core level XPS spectra of indium oxide cubes (a), maize corns (b) and particles (c). O1s core level XPS spectra of indium oxide cubes (d), maize corns (e) and particles (f).

state transformation process are shown in fig.5. In the case of cubes, the original morphology is retained after annealing; but some cracks are formed in the centre of the crystals, possibly due to evolution of H_2O and accompanying weight loss. However, the particles retain the film topography and crystallinity as described above. The different phenomenon is observed in case of maize corn particles where shrinking of the maize corns can be seen by annealing and no cracks were observed in the single corns. This indicates substantially different arrangement of nanorod building blocks to form corn particles. The indium sulphate hydroxide hydrate crystals were transformed into ultrafine indium oxide particles after thermal treatment. The particles look uniform and are 30-40 nm in size. (See fig. S2 for low resolution images)

We further carried out XPS analysis to analyze chemical state of elements and electronic defect structure in indium oxide architectures. The In 3d core level spectra of cubes, corns and particles sample are shown in fig. 6 a, b, c. The spectra are split into spin-orbit doublets ($3d_{5/2}$ and $3d_{3/2}$). This suggests that valency of Indium in the compounds is mainly 3^+.[9] Also the spectra of the different samples look nearly identical, indicating identical nature of In^{3+} in all the three samples. Fig.6 d, e, f shows O1S core-level spectra of the various indium oxide samples. It is clear from the figure that there are two peaks in each of the spectrum; located at at 529.44 and 531.2 eV. The peak at 531.2 is shifted to 531.8 for the particle samples. The peak at 529.44 eV corresponds to oxygen bond in In-O-In while the one at 531.2 is related to oxygen vacancies in the bulk of metal oxide.[9,2f] For all the samples, the relative intensities of the two O1S peaks are significantly different. Especially, for the particle samples, the intensity of the peak due to oxygen vacancies (531.8 eV) is overwhelmingly high, indicating large number of oxygen vacancies. For cubes and corn samples, the ratio of the intensities is 1.38 and 1.30 respectively and that for particle samples is 0.59. This factor has significant effect on photoelectrochemical properties, which is described later in the text.

The optical properties of indium oxide films were studied with Uv-Vis absorption spectroscopy. The Uv-vis spectra of the films are shown in fig.7a. The structureless absorption spectra, as observed here are often encountered in nanostructured films due to size distribution of the particles constituting the film. This causes smearing of the absorption bands near the band-gap energy. Another important reason is the strong electronic coupling in well-interconnected particles.[10] All the three samples show different absorption spectra possibly due to presence of different oxygen vacancies in cubes, maize corns and particles. The band-gaps calculated from graph in fig.7b are 2.84, 2.97 and 3.29 eV for cubes, maize corns and particulate films respectively. The considerable difference in band-gap energy can be explained on the basis of interfacial polaron effect arising from the electron–photon coupling. This effect is favourable for the formation of self trapped exciton from the free exciton attributed to the coexistence of rich oxygen vacancies among the gap.[4b,11]

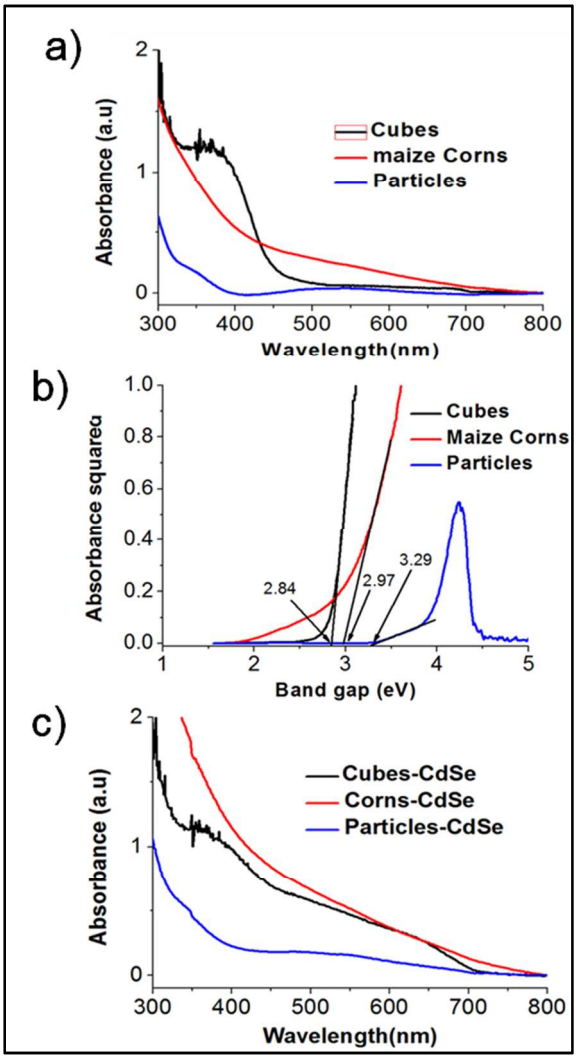

Fig. 7 a) Uv-Vis absorption spectra of indium oxide cubes, maize corns and particles on FTO substrates, b) Calculation of band-gap of indium oxide architectures from Uv-Vis spectra and c) Uv-Vis absorption spectra of indium oxide cubes, maize corns and particles sensitized with CdSe nanoparticles on FTO substrates.

The red shift in absorption spectra of cubes and maize corn particles could be explained by shape prevailing effect over quantum size effect. Similar phenomenon was observed in case of CeO_2 particles.[11b] The direct band gap of In_2O_3 is somewhat controversial, and is reported between 2.3-3.8 eV. Many studies have reported the direct gap of 3.75 eV.[12] Whereas, walsh et.al have reported the band-gap energy of 2.9 eV on the basis of first principle calculations and X-ray spectroscopy.[13] Our group has reported a direct band-gap of 3.05 eV for electrodeposited In_2O_3 spheres,[3a] while Chen et al. reported a band gap of 2.58 eV for In_2O_3 nanoparticles.[14]

Photoluminescence spectra of indium oxide cubes, maize corns and particles are shown in fig. S3. All the three samples show weak emission peaks at 410 and 460 nm with varying intensities. These peaks have commonly been attributed to different sub band-gap energy levels of oxygen vacancies where the electron in the vacancy combines with the hole to emit a photon of corresponding energy.[15] Also the position of the emission peaks; normally reported in the literature, range from 360-640 nm, strongly dependant on the preparation methods.[16] Nanocubes

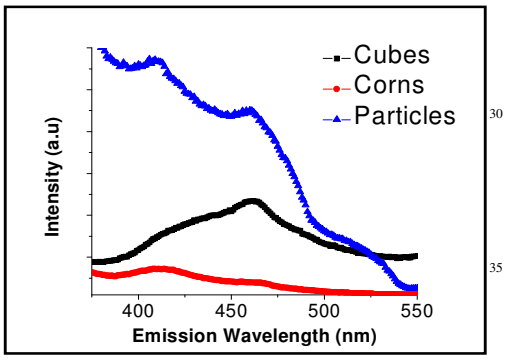

Fig. 8 Room temperature photoluminescence spectra of the indium oxide cubes, maize corns and particle films on FTO substrates. Excitation wavelength was 350 nm.

prepared by electrodeposition method exhibited strong blue emission centered at 405 nm, attributed to singly ionized oxygen vacancies.[2f] In_2O_3 prepared by wet chemical methods exhibit emission peaks between 400-500 nm consistent with our results.[4a,16b]

Despite of favorable band-edge positions, wide band-gap and higher lifetime of injected photoelectrons, there are very few reports on the photosensitization of In_2O_3 and its successful utilization in a photoelectrochemical cells.[6] Motivated by this fact, we decided to photosensitize In_2O_3 with CdSe, a prototypical semiconductor widely used as sensitizer in semiconductor sensitized solar cells. In_2O_3 cubes, maize corns and particles were coated uniformly with CdSe nanoparticles using chemical bath deposition (CBD) technique. For this purpose, our previously described recipe, originally developed by Hodes et.al, which yielded excellent results with photosensitization of ZnO, was used.[5b] Also the results were relatively more reproducible as compared to successive ionic layer adsorption and reaction (SILAR) technique. Nitroltriacetic acid provided consistent results (conformal coating of CdSe), when used as complexing agent instead of commonly used ammonia. For deposition, the films with cubes, maize corns and particles were dipped in deposition solution, as described in the experimental section. After 2.5 h of deposition, the films changed color from faint yellow to blood red indicating the uniform coating of In_2O_3 by CdSe particles. We note that, this deposition time is optimum for obtaining the best photosensitization results. The films were then annealed at 250 °C for 30 min. in ambient air, in order to improve the adhesion between In_2O_3-CdSe layers. The films changed color from blood red to dark brown after annealing, due to quantum confinement effect, arising from increase in crystallite size of CdSe. We found that, annealing step is necessary for improvement of photoelectrochemical properties. Uv-vis spectra of indium oxide films after CdSe deposition are shown in fig.7c. It is clear from the figures that, after deposition, all the films show improved light absorption starting at ~ 700 nm, corresponding to the absorption range of CdSe nanoparticles. It can be also seen that, particles-CdSe films have lowest absorption of all. This is due to lower loading of CdSe on Particulate films. This can be explained on the basis of the fact that, surface bonding characteristics and morphology can have significant

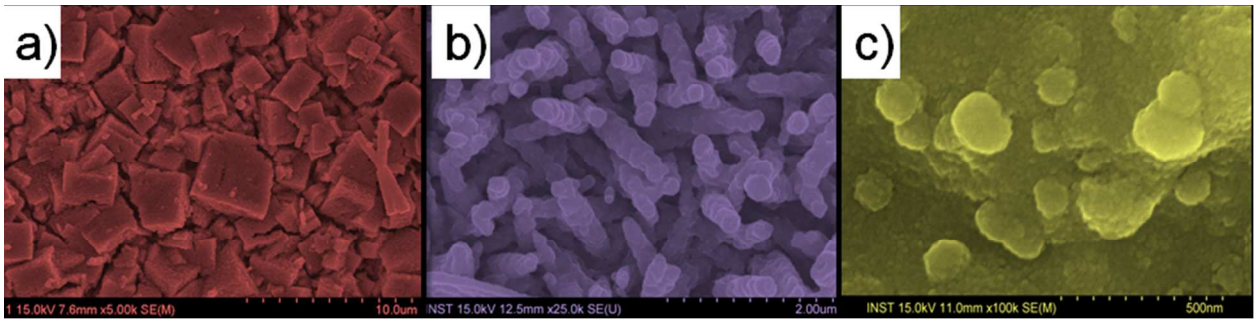

Fig. 9 False colour scanning electron microscope images of the indium oxide cubes, maize corns and particles sensitized with CdSe nanoparticles and annealed at 250 °C on FTO substrates.

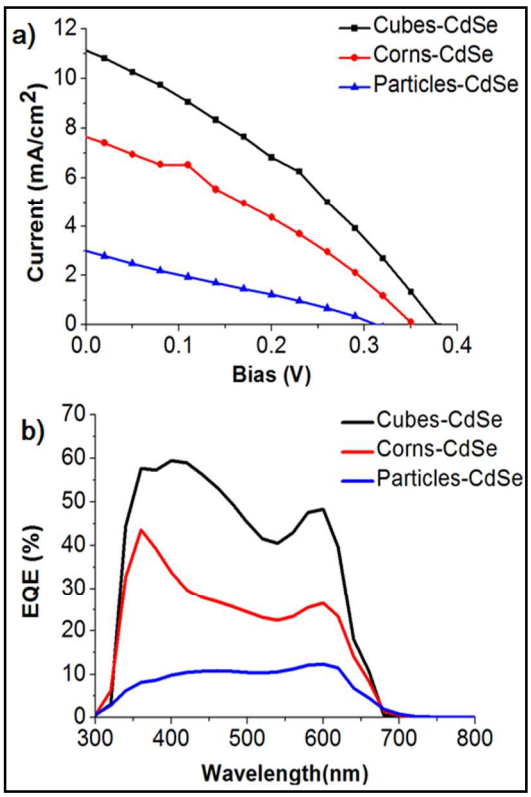

Fig. 10 a) Current-Voltage plots of Indium oxide-CdSe photoelectrochemical cells obtained using platinum as counter electrode and polysulfide as redox shuttle under simulated emission of 1Sun radiation. b) Photocurrent action spectra of the same photoelectrochemical cells.

effect on loading of CdSe particles, as we have observed previously for chemically deposited TiO_2, SnO_2 and ZnO, nanostructures.[5b] SEM images of the samples after CdSe coating and annealing step are shown in fig.9. It can be seen that, all the three samples; cubes, maize corns and particles are uniformly coated with CdSe nanoparticles. In case of maize corns, a well defined core-shell structure of In_2O_3-CdSe is formed, while, the particle samples are uniformly coated with CdSe with some aggregation.

We further measured photoelectrochemical properties of these composite films using Pt-FTO as counter electrode and polysulfide redox electrolyte, as described in detail in experimental section. Fig. 10a shows the current-voltage plots for three systems, obtained under simulated 1 Sun illumination. Cubes-CdSe films showed highest short-circuit current (*Jsc*), open-circuit potential (*Voc*), fill factor (*FF*) and power conversion efficiency (η) values (Table 1). The particulate-CdSe films showed lower values of these photovoltaic parameters, while Corn-CdSe films showed intermediate values. Photocurrent action spectra of the three electrodes, sensitized with CdSe are shown in fig. 10b. The onset of photocurrent for all the samples is around ~700 nm, corresponding to band-gap energy of 1.77 eV. This agrees well with the band gap of CdSe reported in the literature and also indicates that the CdSe particles deposited on various In_2O_3 morphologies have nearly same size.[17] This is considerably different from our previous report regarding ZnO-CdSe system, where the onset of photocurrent was around 750 nm, corresponding to a band-gap energy of 1.66 eV.[5b] This observation points out that, there is substantial difference between growth of CdSe Nanoparticles onto different semiconducting oxides. Also, there is drastic difference between the photocurrent action spectra at ~ 400 nm of ZnO-CdSe and In_2O_3-CdSe system presented here. In case of latter, the EQE value at ~ 400 nm is higher than the former system where the EQE value was declining at the said wavelength. This is possibly due to contribution of In_2O_3 to the overall photocurrent in case of In_2O_3-CdSe system. The drastic difference between the

Table 1 Photovoltaic parameters of In_2O_3-CdSe photoelectrochemical cells extracted from current-voltage plots shown in fig. 9a

Sample	Jsc (mA/cm^2)	Voc (V)	FF	Eff (%)
Cubes-CdSe	11.13	0.37	0.34	1.43
Corns-CdSe	7.64	0.35	0.32	0.87
Particles-CdSe	3.0	0.31	0.26	0.24

photovoltaic parameters of different In_2O_3 samples is obvious and can be readily explained on the basis of morphological difference, oxygen vacancies and interparticle connectivity, which in turn affects the charge transport properties. It is well known fact that, intrinsically, In_2O_3 is an insulator and its semiconducting character depends mainly on defect structure (Oxygen vacancies). In the present case, as determined from XPS measurements, In_2O_3 nanoparticles have highest number of oxygen vacancies, while this number is nearly similar in cubes and corns. These vacancies act as shallow donors near the conduction band, which

increases conductivity and carrier concentration. However, too much number of these vacancies can act as traps and

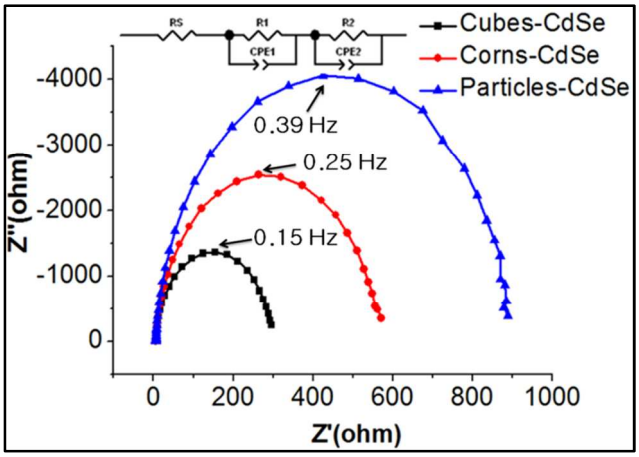

Fig. 11 Nyquist plots of In_2O_3-CdSe photoelectrochemical cells obtained by fitting the original data by an equivalent circuit shown in the inset.

recombination centers.[2f] This fact is also reflected in photoelectrochemical measurements of pristine In_2O_3 samples, in a three electrode cell containing In_2O_3 on FTO as working, Pt as counter and Ag/AgCl (3M NaCl) as a reference electrode (Fig. S4). The electrolyte solution was 1M NaOH. From such measurement, it is possible to study the properties of pristine In_2O_3 electrodes as; the photocurrent generated solely depends on the nature of photoanode and is independent of the quality and catalytic activity of counter electrode. From figure, it is clear that cubes samples show maximum photocurrent (170 μA/cm^2 at 0.1V Vs Ag/AgCl) followed by corn samples (135 μA/cm^2). Particle samples show the lowest photocurrent of 28 μA/cm^2 at 0.1 V. This indicates that, charge generation, separation and transport are efficient in cube samples as compared to maize corns and particle samples. To probe this, we performed impedance spectroscopy measurements on the three samples sensitized with CdSe. Samples for impedance measurements were same as that used in photovoltaic performance measurements. Fig.11 shows the Nyquist plots of the cells obtained by fitting the original data using the equivalent circuit shown in the inset. An impedance spectrum of semiconductor sensitized solar cells shows two semicircles; one in the high frequency region corresponding to the charge transfer resistance (R_1) between counter electrode and electrolyte (Pt-Polysulfide) and the other in low frequency range corresponding to the charge transfer resistance (R_2) in the photoanode (In_2O_3-CdSe).[1c,5b] The size of the second semicircle (the value of R_2) is mainly important factor affecting the photovoltaic parameters, as the factors affecting the R_1 are similar in all the samples. Large differences between the R_2 values can be seen for the cubes, corns and particle samples. The cube samples exhibited smallest R_2 value (~291 ohm) while particle samples showed highest value (~885 ohm). The less value of R_2 means that the photogenerated electrons can easily transport through the photoanode and are collected at FTO without much less chances of recombination. The cube and corn sample show similar nature of oxygen vacancies and consequently similar electronic structure, however the maize corn samples show high resistance to charge transfer (~568.25ohm). This can be explained on the basis of the fact that the charge transfer through the photoanode is affected by interparticle connectivity (grain boundaries) and electronic structure of the transparent oxide. It is clear from the SEM images that the cubes are relatively in more intimate contact with each other, as compared to the corns, thus electrons flowing through the corn

Table 2 Photovoltaic parameters of the photoelectrochemical cells that use indium oxide as transparent n-type oxide as anode with various sensitizers. The data are obtained from the reports published in the literature. Corresponding references are cited in the ref column.

Sample	*Jsc* (mA/cm^2)	*Voc* (V)	FF	Eff (%)	Ref
In_2O_3-CdS	0.04	-	-	-	6a
In_2O_3-In_2S_3	2.9	0.23	0.32	0.21	6b
In_2O_3-N719	3.9	0.41	0.20	0.32	6c
In_2O_3-Ru(II) phenanthroline	3.8	0.29	0.16	0.2	6d
In_2O_3-Mercurochrome	5.35	0.24	0.29	0.38	6e
In_2O_3 (cubes) - CdSe	11.13	0.37	0.34	1.43	Present work

samples may undergo several events of recombination. The highest R_2 value in case of particle sample may be due to combined effect of large number of oxygen vacancies (acting as recombination centers) and lack of interparticle connectivity. The electron lifetime in the composite films (τ_r) can be estimated from maximum frequency of the mid-frequency peak, according to the relation $\tau_r = 1/2\pi f_{max}$, where f_{max} is the maximum frequency of the mid-frequency peak. The f_{max} values for cubes-CdSe, Corns-CdSe and particle-CdSe films are 0.15, 0.25 and 0.39 Hz respectively, which indicates that Cubes-CdSe composite has relatively higher electron lifetime than the other two composites. This is in line with the photovoltaic performance data. The photovoltaic performance obtained in this study (in case of cubes and corn samples) is far better than the values reported in the literature (Table 2). This underlines the importance of careful materials engineering of the morphology and electronic structure of this important n-type oxide. The photovoltaic performance with CdSe sensitization is still lower as compared to TiO_2, SnO_2 and ZnO based devices. Especially *Voc* and *FF* are on the lower side, while *Jsc* is comparable. Careful interface engineering of the In_2O_3 based devices, as has been previously done in the case of other oxides, will certainly improve the photoconversion efficiencies.

Conclusions

Three different morphologies of indium oxide viz. Cubes, maize corns and particles have been fabricated by a soft solution strategy. XPS data shows that particles contain highest number of oxygen vacancies, which are detrimental for the charge transport. After CdSe sensitization, cubes samples showed highest photovoltaic performance, due to presence of optimum number of oxygen vacancies and good interparticle connectivity, which facilitate charge transport through the photoanode. Photocurrent action spectra reveal that CdSe sensitized samples start to generate photocurrent at 700 nm continuing up to 300 nm and In_2O_3 also contributes to the overall photocurrent. The results also

underline the importance of tuning the band-gap, trap states and electronic structure of the transparent oxide. The low temperature and surfactant free method employed here, for direct deposition of In_2O_3 on transparent conducting substrates is scalable for large area depositions and can be used for commercial applications. Furthermore, simply applying the principles of Persons theory, one can tune the morphologies of the formed products obviating the need of any shape directing agents. The highest photovoltaic performance obtained here for In_2O_3 based anodes will certainly boost the studies in the area of this otherwise unexplored semiconductor in photoelectrochemical field. Work is further underway in our lab to control the electronic properties of In_2O_3 by controlling the defect structure and developing the low cost deposition methods to facilitate its use in high performance photoelectrochemical cells.

Acknowledgements

This research was supported by the KIST Institutional Program (2E23964) and also by Basic Science Research Program through the National Research Foundation of Korea (NRF) funded by the Ministry of Education (2013009768). One of the authors (N. K. Shrestha) is supported by The Korean Federation of Science and Technology Societies under Brain Pool program.

Notes and references

[a]*Inorganic Nanomaterials Laboratory, Department of Chemistry, Hanyang University, Seongdong -gu, 133791 Seoul, Republic of Korea. Fax: +82 2 2299-0762; Tel: +82 2-2292-5212; E-mail: shhan@hanyang.ac.kr*

[b]*Centre for Nanomaterials & Energy Devices, School of Physical Sciences, SRTM University, 431606, Nanded, India*

[c]*Energy Storage Research Centre, Korea Institute of Science and Technology, Hwarangno 14-gil 5, Seongbuk-gu, 136791 Seoul, Republic of Korea*

† Electronic Supplementary Information (ESI) available: [Additional SEM images, current-voltage plot and band edge calculations]. See DOI: 10.1039/b000000x/

1 a) D. V. Shinde, R. S. Mane, I.-H. Oh, J. K. Lee and S.-H. Han, *Dalton Trans.*, 2012, 41, 10161; b) S. Muduli, O. Game, V. Dhas, A. Yengantiwar and S. B. Ogale, *Energy Environ. Sci.*, 2011, 4, 2835; c) D. V. Shinde, I. Lim, J. K. Lee, M. M. Sung, R. S. Mane, and S.-H. Han, *J. Mater. Chem. A* , 2013, **1**, 10436; d) J. F. Xie, H. Zhang, S. Li, R. X. Wang, X. Sun, M. Zhou, J. F. Zhou, X. W. Lou and Y. Xie, *Adv. Mater.*, 2013, 25, 5807.

2 a) Y. Li, J. Xu, J. Chao, D. Chen, S. Ouyang, J. Ye and G. Shen, *J. Mater. Chem.*, 2011, 21, 12852; b) D. Caruntu, K. Yao, Z. Zhang, T. Austin, W. Zhou and C. J. O'Connor, *J. Phys. Chem. C*, 2010, 114, 4875; c) S. Elouali, L. G. Bloor, R. Binions, I. P. Parkin, C. J. Carmalt and J. A. Darr, *Langmuir*, 2012, 28, 1879; d) T. Waitz, T. Wagner, T. Sauerwald, C. D. Kohl and M. Tiemann, *Adv. Funct. Mater.*, 2009, 19, 653; e) T. Bielz, H. Lorenz, P. Amann, B. Klotzer and S. Penner, *J. Phys. Chem. C*, 2011, 115, 6622; f) J. Gan, X. Lu, J. Wu, S. Xie, T. Zhai, M. Yu, Z. Zhang, Y. Mao, S. C. I. Wang, Y. Shen and Y. Tong, *Sci. Rep.*, 2013, 3, 1021.

3 a) R. Sharma, R. S. Mane, S. K. Min and S. H. Han, *J. Alloys Compd.*, 2009, 479, 840; b) J. Kane, H. P. Schweizer, *Thin Solid Films*, 1975, **29,** 155; c) W. Lee, J. Lee, H. Lee, W. Yi, S. H. Han, *Appl. Phys. Lett.*, 2007, 91, 043515; d) J. Zai, J. Zhu, R. Qi and X. Qian, *J. Mater. Chem. A*, 2013, **1,** 735; e) F. Quaranta, R. Rella, P. Siciliano, S. Capone, C. Distante, M. Epifani, A. Taurino, *Sens. Actuators, B*, 2002, **84**, 55; f) M. Izaki, *Electrochem. Solid-State Lett*., 1998, **1,** 215; g) O. Bierwagen, J. Speck, *Phys. Status Solidi A*, 2013, DOI: 10.1002/pssa.201330224.

4 a) W. J. Kim, D. Pradhan, Y. Sohn, *J. Mater. Chem. A,* 2013, **1,** 10193; b) Z. Li, P. Zhang, T. Shao, J. Wang, L. Jin, X. Lee, *J. Hazard. Mater.,* 2013, **260,** 40.

5 a) K. Tehare, M. K. Zate, S. S. Bhande, S. A. Patil, S. L. Gaikawad, S. J. Yoon, R. S. Mane, S. H. Lee, S. H. Han, *J. Mater. Chem. A,* 2014, **2**, 478; b) R. S. Mane, D. V. Shinde, S. J. Yoon, S. B. Ambade, J. K. Lee and S.-H. Han, *Appl. Phys. Lett.*, 2012, 101, 033906.

6 a) M. V. Malashchonak, S. K. Poznyak, E. A. Streltsov, A. I. Kulak, O. V. Korolik and A. V. Mazanik, *Beilstein J. Nanotechnol.* 2013, **4,** 255; b) K. Hara, K. Saya and H. Arakawa, *Sol. Energy Mater. Sol. Cells*, 2001, 62, 441; c) S. Mori and A. Asano, *J. Phys. Chem. C*, 2010, 114, 13113; d) K. Hara, H. Sugihara, Y. Tachibana, A. Islam, M. Yanagida, K. Sayama, H. Arakawa, G. Fujihashi and T. Kinoshita, *Langmuir*, 2001, 17, 5992 e) K. Hara, T. Horiguchi, T. Kinoshita, K. Sayama, H. Sugihara and H. Arakawa, *Sol. Energy Mater. Sol. Cells*, 2000, 64, 115

7 R. Pearson, *J. Am. Chem. Soc.*,1963, **85**, 3533

8 X. H. Liu, L. B. Zhou, R. Yi, N. Zhang, R. R. Shi, G. H. Gao and G. Z. Qiu, *J. Phys. Chem.C*, 2008, 112, 18426

9 B. X. Li, Y. Xie, M. Jing, G. X. Rong, Y. C. Tang and G. Z. Zhang, *Langmuir*, 2006, 22, 9380

10 M. V. Artemyev, U. Woggon, H. Jaschinski, L. I. Gurinovich and S. V. Gaponenko, *J. Phys. Chem.*, 2000, 104, 11617

11 a) B. Zou, L. Xiao, T. Li, J. Zhao, Z. Lai, Appl. Phys. Lett., 1991, **59,** 182; b) H. Wu, L. Wang, Catal. Commun., 2011, **12,** 1374.

12 a) A. K. Bal, A. Singh and R. K. Bedi, *Physica B,* 2010, **405,** 3124; b) K. H. L. Zhang, A. Bourlange, R. G. Egdell, S. P. Collins, R. J. Bean, I. K. Robinson and R. A. Cowley, *ACS Nano*, 2012, **6,** 6717.

13 A. Walsh, J. L. F. Da Silva, S. H. Wei, C. Korber, A. Klein, L. F. J. Piper, A. DeMasi, K. E. Smith, G. Panaccione, P. Torelli, D. J. Payne, A. Bourlange and R. G. Egdell, *Phys. Rev. Lett.,* 2008, **100,** 167402.

14 S. F. Chen, X. L. Yu, H. Y. Zhang and W. Liu, *J. Hazard. Mater.,* 2010, **180,** 735.

15 a) W. Yin, J. Su, M. Cao, C. Ni, C. Hu and B. Wei, *J. Phys. Chem. C,* 2010, **114,** 65; b) C. Liang, G. Meng, Y. Lei, F. Phillipp and L. Zhang, *Adv. Mater.,* 2001, **13,** 1330.

16 a) X. Xu and X. Wang, *Inorg. Chem.,* 2009, **48,** 3890; b) F. V. Motta, R. C. Lima, A. P. A. Marques, M. S. Li, E. R. Leite, J. A. Varela and E. Longo, *J. Alloys Compd.,* 2010, **497,** L25.

17 A. L. Rogach, A. Kornowski, M. Y. Gao, A. Eychmüller and H. Weller, *J. Phys. Chem. B*, 1999, 103, 3065.